STAG2 promotes the myelination transcriptional program in oligodendrocytes

Ningyan Cheng[1], Mohammed Kanchwala[2], Bret M. Evers[3], Chao Xing[2,4], Hongtao Yu[1,5,6,7,*]

[1]Department of Pharmacology, University of Texas Southwestern Medical Center, Dallas, TX 75390, USA.

[2]Eugene McDermott Center for Human Growth and Development, University of Texas Southwestern Medical Center, Dallas, TX 75390, USA.

[3]Division of Neuropathology, University of Texas Southwestern Medical Center, Dallas, TX, 75390, USA.

[4]Department of Bioinformatics, Department of Population and Data Sciences, University of Texas Southwestern Medical Center, Dallas, TX 75390, USA.

[5]Westlake Laboratory of Life Sciences and Biomedicine, Hangzhou, China.

[6]School of Life Sciences, Westlake University, Hangzhou, China.

[7]Institute of Biology, Westlake Institute for Advanced Study, Hangzhou, China.

[*]Correspondence: yuhongtao@westlake.edu.cn

SUMMARY

Cohesin folds chromosomes via DNA loop extrusion. Cohesin-mediated chromosome loops regulate transcription by shaping long-range enhancer-promoter interactions, among other mechanisms. Mutations of cohesin subunits and regulators cause human developmental diseases termed cohesinopathy. Vertebrate cohesin consists of SMC1, SMC3, RAD21, and either STAG1 or STAG2. To probe the physiological functions of cohesin, we created conditional knockout (cKO) mice with *Stag2* deleted in the nervous system. *Stag2* cKO mice exhibit growth retardation, neurological defects, and premature death, in part due to insufficient myelination of nerve fibers. *Stag2* cKO oligodendrocytes exhibit delayed maturation and downregulation of myelination-related genes. *Stag2* loss reduces promoter-anchored loops at downregulated genes in oligodendrocytes. Thus, STAG2-cohesin generates promoter-anchored loops at myelination-promoting genes to facilitate their transcription. Our study implicates defective myelination as a contributing factor to cohesinopathy and establishes oligodendrocytes as a relevant cell type to explore the mechanisms by which cohesin regulates transcription.

INTRODUCTION

Chromosomes in a single human diploid cell, if linearly stitched together, span a length of more than two meters. They need to be properly folded to be housed in the cell nucleus with a diameter of 10 μm. Chromosome folding occurs in a dynamic, structured way that regulates gene expression, and DNA replication and repair. Initially discovered as the molecular glue that tethers sister chromatids for segregation during mitosis (Haarhuis et al., 2014; Uhlmann, 2016; Yatskevich et al., 2019; Zheng and Yu, 2015), the cohesin complex has later been shown to be critical for structured chromosome folding and gene expression (Haarhuis et al., 2017; Rao et al., 2017; Schwarzer et al., 2017; Wutz et al., 2017).

Cohesin is loaded on chromosomes by the cohesin loader NIPBL. The cohesin–NIPBL complex can extrude DNA loops bi-directionally in an ATP-dependent manner (Davidson et al., 2019; Kim et al., 2019; Vian et al., 2018). The chromatin insulator CTCF has been proposed to block loop extrusion by cohesin, establishing topologically associated domains (TADs) and marking TAD boundaries. Chromatin interactions within each TAD are favored whereas inter-TAD interactions are disfavored. Thus, chromosome loops and TADs shape long-range cis-element interactions, such as promoter-enhancer interactions, thereby regulating transcription.

The vertebrate cohesin complex contains four core subunits: the SMC1–SMC3 heterodimeric ATPase, the kleisin subunit RAD21 that links the ATPase heads, and the HEAT-repeat protein STAG1 or STAG2. STAG1 and STAG2 bind to RAD21 in a mutually exclusive manner and create docking sites for several regulatory proteins, including CTCF (Hara et al., 2014; Li et al., 2020). STAG1 and STAG2 also interact with DNA and the SMC1–SMC3 hinge domains (Shi et al., 2020). STAG1 and STAG2 play redundant roles in sister-chromatid cohesion in

cultured human cells, as both need to be simultaneously depleted to produce overt cohesion defects (Hara et al., 2014).

Mutations of NIPBL and cohesin subunits, including STAG2, result in human developmental diseases termed cohesinopathies, which affect multiple organs and systems (Remeseiro et al., 2013b; Soardi et al., 2017). In patients with cohesinopathies, mental retardation and neurological abnormalities caused by brain development defects are common (Piche et al., 2019). Dysregulation of gene transcription as a result of reduced cohesin functions has been suggested to underlie these developmental defects (De Koninck and Losada, 2016; Remeseiro et al., 2013a). In addition, several cohesin genes, including *STAG2*, are frequently mutated in a variety of human cancers (Martincorena and Campbell, 2015).

To better understand the physiological roles of cohesin, we deleted *Stag2* specifically in the nervous system in the mouse. The *Stag2* conditional knockout (cKO) mice exhibited deficient myelination. Loss of STAG2 delayed the maturation of oligodendrocytes and reduced chromosome loops in oligodendrocytes and impaired the transcription of myelination-related genes. Our findings establish the requirement for cohesin in proper gene expression in specific cell types and implicate defective myelination as a potential contributing factor to cohesinopathy.

RESULTS

Stag2 ablation in the nervous system causes growth retardation and neurological defects

Stag1 is required for mammalian embryonic development (Remeseiro et al., 2012), indicating that *Stag2* cannot compensate for the loss of *Stag1*. To examine the roles of *Stag2* during development in the mouse, we targeted a critical exon (exon 8) of *Stag2*, which is located on the X chromosome, using CRISPR-Cas9 (Figure S1A). The $Stag2^{null}$ embryos showed severe developmental defects and underwent necrosis by E11.5 days (Figure S1B). Thus, *Stag2* is required for mouse embryonic development, consistent with a recent report (De Koninck et al., 2020). *Stag1* and *Stag2* have non-redundant developmental functions.

Because whole-body knockout of *Stag2* caused embryonic lethality, we created a *Stag2* "floxed" mouse line ($Stag2^{f/f}$) by homologous recombination with a template that contained two LoxP sites flanking exon 8 (Figure S2A,B). To study the physiological function of STAG2 in adult mice, we crossed the $Stag2^{f/f}$ mice with mice bearing the *Ert2-Cre* genomic insertion and generated $Stag2^{f/y}$*;Ert2-Cre* progenies. The $Stag2^{f/y}$*;Ert2-Cre* adult mice were injected with tamoxifen to induce *Stag2* deletion in the whole body (Figure S2C). Genotyping analysis of blood extracts showed that tamoxifen induced efficient disruption of the *Stag2* gene locus in $Stag2^{f/y}$*;Ert2-Cre* mice (Figure S2D,E). These *Stag2*-deficient adult mice did not show early onset of spontaneous tumor formation, indicating that *Stag2* mutation alone in somatic cells of mice is insufficient to induce tumorigenesis. The *Stag2*-deficient mice also did not have other obvious adverse phenotypes (Figure S2F), except that they had slightly lower body weight (Figure S2G,H), probably due to tissue homeostasis alterations recently reported by others (De Koninck et al., 2020).

STAG2 mutations are found in human cohesinopathy patients with mental retardation and neuropsychiatric behaviors (Soardi et al., 2017). To study the function of STAG2 in the nervous system, we generated *Stag2* conditional knockout mice (*Stag2* cKO) by crossing *Stag2*$^{f/f}$ mice with *Nestin-Cre* mice (Giusti et al., 2014) (Figure 1A,B). The progenies were born in the Mendelian ratio, but *Stag2*$^{f/y}$*;Cre* pups presented growth retardation and premature death (Figure 1C-E). More than 50% *Stag2*$^{f/y}$*;Cre* mice died aged about 3 weeks while the rest died at about 4 months. *Stag2*$^{f/y}$ mice did not show differences discernible from WT littermates. Although *Stag2*$^{f/y}$*;Cre* mice did not present microcephaly, they exhibited frequent hydrocephaly that might contribute to their premature death. The *Stag2*$^{f/y}$*;Cre* mice displayed normal drinking and feeding behaviors (Figure 1F,G), but showed reduced plasma IGF-1 levels compared to the control mice (Figure 1H). *Stag2*$^{f/y}$*;Cre* mice showed forepaw and hindlimb clasping (Figure 1I) and limb tremors (Movie 1), which were not seen in *Stag2*$^{f/y}$ mice. These data indicate that *Stag2* deficiency in the nervous system causes growth retardation and neurological defects.

Stag2 ablation causes hypomyelination

Hematoxylin and eosin staining of brain sections of *Stag2*$^{f/y}$*;Cre* mice did not reveal overt anatomical defects (Figure S3A). To understand the origins of neurological defects caused by *Stag2* deletion, we analyzed the gene expression changes in *Stag2*$^{f/y}$*;Cre* mouse brains by RNA-sequencing (RNA-seq) (Figure 2A). Compared with the control groups, 105 and 62 genes were significantly downregulated or upregulated by more than two folds, respectively, in the *Stag2*-deficient brains. The decreased expression of top differentially expressed genes (DEGs) was confirmed by reverse transcription quantitative PCR (RT-qPCR) (Figure 2B). Among the 105 downregulated DEGs in the brains of *Stag2* cKO mice, 44 were enriched in myelin (Figure 2C)

(Thakurela et al., 2016). The Ingenuity Pathway Analysis (IPA) pinpoints cholesterol biosynthesis pathways as the most affected canonical pathways (Figure 2D). We further confirmed that the cholesterol biosynthesis precursors were reduced in *Stag2$^{f/y}$;Cre* brains (Figure S3B).

Myelin is the membrane sheath that wraps around axons to facilitate rapid nerve conduction and maintain metabolic supply (Williamson and Lyons, 2018). Dynamic myelination in the central nervous system (CNS) is critical for proper neurodevelopment, and defective myelination is associated with autoimmune and neurodegenerative diseases (Mathys et al., 2019; Wolf et al., 2021). As cholesterol biosynthesis is essential for normal myelination (Hubler et al., 2018; Saher et al., 2005), we hypothesized that depletion of STAG2 caused myelination defects in the nervous system.

Indeed, brain sections of *Stag2$^{f/y}$;Cre* mice showed greatly reduced luxol fast blue (LFB) staining compared to those of *Stag2$^{f/y}$* and *Nestin-Cre* heterozygous mice (Figure 3A and S4A). Immunohistochemistry using antibodies against myelin proteins, MBP and PLP1, confirmed that *Stag2* cKO mice had significant defects in myelin fiber formation (Figure 3B-F). In both cerebral cortex and cerebellum, there were fewer and sparser myelin fibers in *Stag2$^{f/y}$;Cre* mice, as compared to the *Stag2$^{f/y}$* controls. Axon myelin ensheathment was further examined using transmission electron microscopy (Figure 3G). *Stag2$^{f/y}$;Cre* mice had significantly fewer myelin-wrapped axons at optic nerves. Collectively, these data indicate insufficient myelination in the *Stag2* cKO mice. Myelination predominantly occurs at 3 weeks after birth in the mouse. The timing of premature death of *Stag2* cKO mice is thus consistent with defective myelination as a contributing factor to the lethality.

STAG2 regulates transcription in OLs

We examined *Stag1* and *Stag2* expression patterns in wild-type mouse brains by *in situ* hybridization using isotope-labeled RNA probes (Figure S4B). Both *Stag1* and *Stag2* were expressed at high levels in hippocampus, medial habenula, neocortex, and cerebellum granular layer. Aside from these regions, the *Stag2* transcripts were detected at relatively high levels in subventricular zone, thalamus, fiber tracts, midbrain, and hindbrain regions. *Stag2* is thus ubiquitously expressed in the brain.

Oligodendrocytes (OLs) are responsible for myelination in the CNS. To examine whether the OL lineage was affected by *Stag2* deletion, we performed single-cell RNA sequencing (scRNA-seq) analysis of $Stag2^{f/y};Cre$ and $Stag2^{f/y}$ forebrains. As revealed by clusters in the t-SNE plot, the two genotype groups had similar cellular compositions (Figure 4A,B). All cell clusters were present in $Stag2^{f/y};Cre$ brains, indicating generally normal neural cell differentiation. Cell-type identities were discovered with feature gene expression (Figure S5A). The OL lineage consisted of five clusters: cycling OL progenitors (OPCcycs), OL progenitors (OPCs), newly formed OLs (NFOLs), myelin-forming OLs (mFOLs), and fully matured OLs (MOLs). Quantification of the distributions of these five cell types within the OL lineage revealed a mild reduction in the number of MOLs in $Stag2^{f/y}$ forebrains (Figure 4C). We noticed that a higher percentage of neurons was recovered in the $Stag2^{f/y};Cre$ group. Since the bulk RNA-seq results did not show global upregulation of neuron-specific genes, we suspect that neurons in $Stag2^{f/y};Cre$ had fewer myelin-wrapped axons and were easier to be dissociated and kept alive during our library preparation for scRNA-seq. Thus, from the transcriptome analysis, we did not observe overt defects in most neural cell differentiation in the *Stag2*-deficient forebrain regions.

We then performed trajectory inference and pseudotime analysis of the OL lineage (Figure S5B,C). Consistent with our cell-type assignment, pseudotime variables indicated continuous

differentiation from OPCs to NFOLs, mFOLs, and MOLs (Figure S5D,E). The re-clustering of single cells in the OL lineage along the pseudotime path revealed that more cells were present in the terminal maturation stages in the *Stag2*$^{f/y}$ brains (Figure S5F,G). Conversely, more cells were retained at the undifferentiated stages in the *Stag2*$^{f/y}$*;Cre* brains. Strikingly, some myelination genes, including *Mal*, were specifically repressed in *Stag2*$^{f/y}$*;Cre* MOLs, with their expression in non-neural cells unaltered (Figures 4D and S6A). These observations suggest that STAG2 deficiency delays the maturation of OLs and compromises myelination-specific gene expression in mature OLs. Interestingly, compared to *Stag2* and genes encoding other cohesin core subunits, *Stag1* transcripts are less abundant in the OL lineage, except for cycling OPCs (Figure S6B,C). The low expression of *Stag1* in mature OLs might make these cells more dependent on *Stag2* for function.

To confirm the transcriptional defects in the OL lineage caused by *Stag2* deletion, we isolated primary OLs at intermediate differentiation stages from *Stag2*$^{f/y}$*;Cre* and *Stag2*$^{f/y}$ forebrains with antibody-conjugated magnetic beads and conducted bulk RNA-seq analysis (Figure 4E). For both genotypes, the marker genes for NFOL and mFOLs were highly expressed in the isolated primary OLs (Figure S7A), suggesting that they mainly contained these two cell types. In *Stag2*-deleted OLs, 271 and 292 genes were downregulated or upregulated by more than two folds, respectively (Figure 4F). The top canonical pathway enriched in these DEGs was the cholesterol biosynthesis pathway (Figure 4G). Intriguingly, the downregulated genes were generally highly expressed in WT cells, whereas the upregulated genes had low expression levels in WT cells (Figure S7B-D). Among the 105 downregulated DEGs identified by RNA-seq analysis of the whole brain of *Stag2*-deficient mice, 42 were also differentially expressed in primary oligodendrocytes (Figure 4H). The cholesterol biosynthesis pathways were recognized as

the major altered pathways (Figure S7E). Thus, defective cholesterol biosynthesis likely underlies hypomyelination and neurological defects in *Stag2* cKO mice.

We performed chromatin immunoprecipitation sequencing (ChIP-seq) experiments to examine the enrichment of the active transcription mark H3K27ac in *Stag2*$^{f/y}$ and *Stag2*$^{f/y}$*;Cre* OLs and found that *Stag2* loss did not appreciably affect H3K27Ac enrichment at transcription start sites (TSS) (Figure S8A,B). Consistent with our RNA-seq results, the upregulated genes had much lower H3K27ac enrichment near their TSS, indicating that they were less active. We then checked the genomic distribution of STAG2 by ChIP-seq. Among other genomic loci, STAG2 was enriched at TSS of stable and downregulated genes, including genes in the cholesterol biosynthesis pathways (Figure S8C,D). It was enriched at the TSS of upregulated genes to a lesser extent, suggesting that *Stag2* loss might have indirectly affected the expression of these less active genes.

Stag2 deletion does not alter compartments or TADs in OLs

To investigate whether chromosome conformation was altered by *Stag2* deletion and whether that caused transcription dysregulation, we performed high-dimensional chromosome conformational capture (Hi-C) analysis of primary OLs isolated from *Stag2*$^{f/y}$ and *Stag2*$^{f/y}$*;Cre* mice. We observed few compartment switching events in *Stag2*-deleted cells (Figure 5A-C and S9A-C). Virtually all genomic regions in *Stag2*-deleted cells were kept in their original compartment categories (AA or BB) (Figure 5C). Only a very small number of genomic regions switched compartments (AB or BA). Consistent with the RNA-seq data, analysis of average gene expression changes of DEGs in these genomic regions revealed that more genes located in the transcriptionally active A compartment (AA) were repressed in *Stag2*-deleted cells and more genes in the transcriptionally silent B compartment (BB) were upregulated (Figure 5D and S9D). Genes that switched from the

A compartment to the B compartment were not more repressed compared to those that remained in the A compartment. Likewise, compared to genes that stayed in the B compartment, genes located in chromatin regions that switched from compartment B to A were not significantly activated. Acute depletion of all forms of cohesin eliminates TAD formation (Wutz et al., 2017). In contrast, deletion of *Stag2* had minimal impact on TAD formation in oligodendrocytes (Figure 5E-H, S9E,F), suggesting that STAG1-cohesin compensates for the loss of STAG2-cohesin in spatial organization of chromatin at larger than megabase scales. Therefore, our findings are inconsistent with compartment switching and TAD alterations being the underlying cause for the observed gene expression changes in STAG2-deficient OLs.

Promoter-anchored loops were reduced in *Stag2*-deleted OLs

While TAD boundaries are largely conserved among species and cell types, chromatin interactions within each TAD are more flexible and variable in cells undergoing differentiation, tumorigenesis, and reprogramming (Dixon et al., 2015; Dixon et al., 2012). Among the intra-TAD chromatin interactions, the enhancer-promoter loops are particularly important for transcription and are often cell-type specific. We examined whether chromatin loops in OLs were affected by *Stag2* loss. Compared to *Stag2*$^{f/y}$ OLs, *Stag2*$^{f/y}$*;Cre* OLs had significantly fewer loops across almost all genomic distances (Figure 6A,B and S10). Loops specific to *Stag2*$^{f/y}$*;Cre* OLs, which were likely mediated by STAG1-cohesin, were longer than STAG2-dependent *Stag2*$^{f/y}$-specific loops. When genomic distances exceeded 0.25 Mb, the loops from *Stag2*$^{f/y}$*;Cre* cells gradually gained higher scores over loops from *Stag2*$^{f/y}$ cells (Figure 6C). Therefore, STAG1-cohesin cannot completely compensate for STAG2-cohesin during loop formation. STAG1-cohesin-mediated loops are

relatively longer than STAG2-cohesin-mediated loops, consistent with published findings in HeLa cells (Wutz et al., 2020).

We then tested whether the loop number decrease in *Stag2*-deficient cells could be a cause for transcriptional changes. When examining the local Hi-C maps, we noticed that loops anchored at gene promoters, including those of downregulated genes, were reduced in *Stag2$^{f/y}$;Cre* oligodendrocytes (Figure 6D and S11). Promoter-anchored loops (P-loops) can potentially be promoter-promoter links, promoter-enhancer links, and gene loops. The total number of P-loops was proportionally decreased in *Stag2$^{f/y}$;Cre* cells (Figure S12A). Moreover, the loops anchored at the downregulated genes were stronger than those at upregulated and stable genes (Figure S12B). We then compared P-loops associated with DEGs using pileup analysis of local contact maps. Loop enrichment at promoters of downregulated genes was reduced in *Stag2$^{f/y}$;Cre* cells to a greater extent than that at promoters of upregulated and stable genes (Figure 6E). Taken together, our results suggest that *Stag2* loss diminishes short chromosome loops, including promoter-anchored loops. Highly expressed genes might be more reliant on these loops for transcription and are preferentially downregulated by *Stag2* loss.

We also performed pileup analysis of local chromatin regions flanking transcription start sites (TSS) (Figure 6F). Strikingly, we observed a clear stripe that extended from the TSS of downregulated gene only in the direction of transcription. The formation of promoter-anchored stripes (P-stripes) on aggregated plots is consistent with one-sided loop extrusion from the promoter to the gene body. The P-stripe was still present in *Stag2$^{f/y}$;Cre* cells, suggesting that STAG1 could compensate for the loss of STAG2 and mediate its formation (Figure 6F and S12C).

DISCUSSION

Cohesin is critical for the three-dimensional (3D) organization of the genome by extruding chromosome loops. Acute depletion of cohesin abolishes chromosome loops and TADs, but has moderate effects on transcription. The two forms of cohesin in vertebrate somatic cells, namely STAG1-cohesin and STAG2-cohesin, have largely redundant functions in supporting sister-chromatid cohesion and cell viability, but they have non-redundant functions during development. In this study, we have established a myelination-promoting function of STAG2 in the central nervous system (CNS) in the mouse. We further provide evidence linking hypomyelination caused by STAG2 loss to reduced promoter-anchored loops at myelination genes in oligodendrocytes.

Myelination functions of STAG2 and implications for cohesinopathy

Selective ablation of *Stag2* in the nervous system in the mouse causes growth retardation, neurological defects, and premature death. STAG2 loss delays the maturation of oligodendrocytes and reduces the expression of highly active myelin and cholesterol biosynthesis genes in oligodendrocytes, resulting in hypomyelination in the CNS. Hypomyelination disorders in humans and mice are known to produce abnormal neurological behaviors similar to those seen in our *Stag2* cKO mice, suggesting that hypomyelination is a major underlying cause for the phenotypes in *Stag2* cKO mice. The growth retardation in these mice can be explained by insufficient secretion of growth hormones, which may be a consequence of defective neuronal signaling.

Mutations of cohesin subunits and regulators, including STAG2, cause the Cornelia de Lange syndrome (CdLS) and other similar developmental diseases, collectively termed cohesinopathy. CdLS patients exhibit short stature and developmental defects in multiple tissues

and organs, including the brain. Although STAG2 mutations are implicated in human cohesinopathy, these mutations are rare and hypomorphic (Soardi et al., 2017). The cohesin loader NIPBL is the most frequently mutated cohesin regulator in cohesinopathy (Mannini et al., 2013). NIPBL deficiency is expected to affect the functions of both STAG1- and STAG2-cohesin. It is possible that the partial loss of STAG2-cohesin function leads to subtle myelination defects in patients with cohesinopathy. Indeed, lack of myelination in certain brain regions of CdLS patients has been reported (Avagliano et al., 2017; Vuilleumier et al., 2002). As myelination of the CNS mostly occurs after birth and during childhood, strategies aimed at enhancing myelination might help to alleviate certain disease phenotypes and symptoms.

Mechanisms by which STAG2 promotes myelination

STAG2 promotes oligodendrocyte maturation and the expression of myelination genes in mature oligodendrocytes. Because STAG2 does not have an established cohesin-independent function, it most likely activates the myelination-promoting transcriptional program as a core component of cohesin. Consistent with previous reports (Rao et al., 2017), loss of STAG2-cohesin in oligodendrocytes does not affect genome compartmentalization, but reduces the number of relatively short chromosome loops, including promoter-anchored loops. Promoter-anchored loops at downregulated genes are reduced to a greater extent than those at stable and upregulated genes. These findings suggest that STAG2-cohesin promotes the myelination transcriptional program by forming promoter-anchored loops.

Pileup analysis of Hi-C maps reveals the formation of asymmetric promoter-anchored stripes in the direction of transcription at downregulated genes, indicative of active loading of cohesin at transcription start sites followed by one-sided loop extrusion from the promoter to the

gene body. The stripes are, however, not reduced in STAG2-deficient cells. Because both forms of cohesin are capable of loop extrusion, it is possible that STAG1-cohesin can compensate for the loss of STAG2-cohesin in loop extrusion. It remains to be tested whether the intrinsic kinetics and processivity of loop extrusion mediated by the two forms of cohesin are differentially regulated by cellular factors or posttranslational modifications and whether these differences contribute to their non-redundant roles in transcription regulation.

We envision three possibilities that may account for why oligodendrocytes, but not other cell types, are more severely affected by *Stag2* loss in the CNS. First, STAG2-cohesin may be more abundant than STAG1-cohesin in post-mitotic OLs, making them more dependent on STAG2 for proper functions. Second, STAG1-cohesin preferentially localizes to CTCF-enriched TAD boundaries whereas STAG2-cohesin is more enriched at enhancers lacking CTCF (Kojic et al., 2018). Enhancers are critical for cell-type-specific gene transcriptional programs. To cooperate with the axonal growth during postnatal neurodevelopment, enhancer-enriched transcription factors induce timely and robust gene expression in oligodendrocytes for proper myelination (Mitew et al., 2014). The high-demand for enhancer function may render the transcription of myelination genes more reliant on STAG2-cohesin. Finally, the C-terminal regions of STAG1 and STAG2 are divergent in sequence and may bind to different interacting proteins and be subjected to differential regulation. STAG2 may interact with oligodendrocyte-specific transcription factors and be preferentially recruited to myelination genes. It will be interesting to investigate the interactomes of STAG1 and STAG2 in oligodendrocytes using mass spectrometry.

STAG2-mediated chromosome looping and transcription

The mechanisms by which STAG2-dependent chromosome looping facilitates transcription are unclear at present. We propose several models that are not mutually exclusive (Figure 7). First, by forming promoter-enhancer loops, STAG2-cohesin brings the mediator complex and other enhancer-binding factors to the spatial proximity of the general transcriptional machinery at the promoter, thereby enhancing RNA polymerase II recruitment and transcription initiation. The existence of P stripes at STAG2-dependent genes in the Hi-C maps suggests that STAG2-mediated promoter-enhancer loops may involve enhancers located in the gene body. Second, loop extrusion by STAG2-cohesin may promote transcription elongation by regulating transcription-coupled pre-mRNA processing. For example, STAG2 has been shown to interact with RNA-DNA hybrid structures termed R-loops *in vitro* and in cells (Pan et al., 2020; Porter et al., 2021). R-loops formed between the nascent pre-mRNA and the DNA template impede transcription elongation and need to be suppressed (Moore and Proudfoot, 2009). When traveling with the transcription machinery on DNA, STAG2-cohesin might directly suppress R-loop formation or recruit other factors, such as the spliceosome, for co-transcriptional pre-mRNA processing and R-loop resolution. Third, STAG2-cohesin may establish promoter-terminator gene loops to recycle the RNA polymerase II that has finished one cycle of transcription back to the transcription start site for another round of transcription. Future experiments using high-resolution Hi-C methods in oligodendrocytes will allow us to better define the nature of STAG2-dependent promoter-anchored loops and stripes. It will also be interesting to examine whether *Stag2* deletion causes the accumulation of R-loops in downregulated genes and the incomplete splicing of their pre-mRNAs.

CONCLUSION

We have discovered a requirement for the cohesin subunit STAG2 in the myelination of the central nervous system in mammals. Our findings implicate hypomyelination as a contributing factor to certain phenotypes of cohesinopathy, including growth retardation and neurological disorders. We provide evidence to suggest that STAG2 promotes the myelination transcriptional program in oligodendrocytes through the formation of promoter-anchored loops. Our study establishes oligodendrocytes as a physiologically relevant cell system for dissecting the cellular functions and regulatory mechanisms of cohesin-mediated chromosome folding and genome organization.

STAR★METHODS

Detailed methods are provided in the online version of this paper and include the following:

- KEY RESOURCES TABLE
- RESOURCE AVAILABILITY
  - Lead contact
  - Materials availability
  - Data and code availability
- EXPERIMENTAL MODEL AND SUBJECT DETAILS
  - Generation of *Stag2*$^{f/f}$ and *Stag2*$^{f/y}$ mice and mouse husbandry
- METHOD DETAILS
  - Immunoblotting
  - Tissue histology and immunohistochemistry
  - Isolation of primary oligodendrocytes
  - TSE Metabolic cages analysis
  - Growth hormone and IGF-1 detection.
  - Sterol and oxysterol composition analysis
  - Electron Microscopy
  - Generation of RNA-seq libraries and sequencing
  - Differential expression and pathway analysis
  - RT-qPCR analysis
  - Transcriptional profiling of brain cells
  - ChIP-seq
  - Hi-C libraries generation and sequencing

SUPPLEMENTAL INFORMATION

Supplemental information can be found online.

ACKNOWLEDGMENTS

We thank Sung Jun Bae for taking the mouse photos and John Shelton for help with histology and *in situ* hybridization. We are grateful to Jeffrey McDonald for the sterol composition analysis, Richard Lu and Lu Sun for providing reagents and advice for oligodendrocytes isolation, and Applied Bioinformatics Laboratories at NYU Langone Health for the Hi-C analysis. We also thank the Yu lab members for helpful discussions and for reading the manuscript critically. This study was supported by the Cancer Prevention and Research Institute of Texas (CPRIT) (RP160667-P2) and the Welch foundation (I-1441).

AUTHOR CONTRIBUTIONS

N.C. and H.Y. conceived and designed the study. N.C. performed all the experiments. M.K., N.C., and C. X. performed the analysis and interpretation of NGS data. N.C. and B.M.E. performed histology and EM image analysis. N.C. and H.Y. wrote the manuscript with input from all authors. H.Y. supervised the project. All authors approved the manuscript.

DECLARATION OF INTERESTS

The authors declare no competing interests.

REFERENCES

Andrews, S. (2010). FastQC: a quality control tool for high throughput sequence data.

Avagliano, L., Grazioli, P., Mariani, M., Bulfamante, G.P., Selicorni, A., and Massa, V. (2017). Integrating molecular and structural findings: Wnt as a possible actor in shaping cognitive impairment in Cornelia de Lange syndrome. Orphanet J. Rare Dis. *12*, 174.

Ay, F., Bailey, T.L., and Noble, W.S. (2014). Statistical confidence estimation for Hi-C data reveals regulatory chromatin contacts. Genome Res *24*, 999-1011.

Butler, A., Hoffman, P., Smibert, P., Papalexi, E., and Satija, R. (2018). Integrating single-cell transcriptomic data across different conditions, technologies, and species. Nat Biotechnol *36*, 411-420.

Cahoy, J.D., Emery, B., Kaushal, A., Foo, L.C., Zamanian, J.L., Christopherson, K.S., Xing, Y., Lubischer, J.L., Krieg, P.A., Krupenko, S.A.*, et al.* (2008). A transcriptome database for astrocytes, neurons, and oligodendrocytes: a new resource for understanding brain development and function. J Neurosci *28*, 264-278.

Cao, J., Spielmann, M., Qiu, X., Huang, X., Ibrahim, D.M., Hill, A.J., Zhang, F., Mundlos, S., Christiansen, L., Steemers, F.J.*, et al.* (2019). The single-cell transcriptional landscape of mammalian organogenesis. Nature *566*, 496-502.

Choi, E., Zhang, X., Xing, C., and Yu, H. (2016). Mitotic Checkpoint Regulators Control Insulin Signaling and Metabolic Homeostasis. Cell *166*, 567-581.

Davidson, I.F., Bauer, B., Goetz, D., Tang, W., Wutz, G., and Peters, J.M. (2019). DNA loop extrusion by human cohesin. Science *366*, 1338-1345.

De Koninck, M., Lapi, E., Badia-Careaga, C., Cossio, I., Gimenez-Llorente, D., Rodriguez-Corsino, M., Andrada, E., Hidalgo, A., Manzanares, M., Real, F.X.*, et al.* (2020). Essential Roles

of Cohesin STAG2 in Mouse Embryonic Development and Adult Tissue Homeostasis. Cell Rep. *32*, 108014.

De Koninck, M., and Losada, A. (2016). Cohesin Mutations in Cancer. Cold Spring Harb Perspect Med *6*.

Dixon, J.R., Jung, I., Selvaraj, S., Shen, Y., Antosiewicz-Bourget, J.E., Lee, A.Y., Ye, Z., Kim, A., Rajagopal, N., Xie, W.*, et al.* (2015). Chromatin architecture reorganization during stem cell differentiation. Nature *518*, 331-336.

Dixon, J.R., Selvaraj, S., Yue, F., Kim, A., Li, Y., Shen, Y., Hu, M., Liu, J.S., and Ren, B. (2012). Topological domains in mammalian genomes identified by analysis of chromatin interactions. Nature *485*, 376-380.

Dobin, A., Davis, C.A., Schlesinger, F., Drenkow, J., Zaleski, C., Jha, S., Batut, P., Chaisson, M., and Gingeras, T.R. (2013). STAR: ultrafast universal RNA-seq aligner. Bioinformatics *29*, 15-21.

Dulken, B.W., Buckley, M.T., Navarro Negredo, P., Saligrama, N., Cayrol, R., Leeman, D.S., George, B.M., Boutet, S.C., Hebestreit, K., Pluvinage, J.V.*, et al.* (2019). Single-cell analysis reveals T cell infiltration in old neurogenic niches. Nature *571*, 205-210.

Durand, N.C., Shamim, M.S., Machol, I., Rao, S.S., Huntley, M.H., Lander, E.S., and Aiden, E.L. (2016). Juicer Provides a One-Click System for Analyzing Loop-Resolution Hi-C Experiments. Cell Syst. *3*, 95-98.

Flores-Obando, R.E., Freidin, M.M., and Abrams, C.K. (2018). Rapid and Specific Immunomagnetic Isolation of Mouse Primary Oligodendrocytes. J. Vis. Exp.

Flyamer, I.M., Illingworth, R.S., and Bickmore, W.A. (2020). Coolpup.py: versatile pile-up analysis of Hi-C data. Bioinformatics *36*, 2980-2985.

Giusti, S.A., Vercelli, C.A., Vogl, A.M., Kolarz, A.W., Pino, N.S., Deussing, J.M., and Refojo, D. (2014). Behavioral phenotyping of Nestin-Cre mice: implications for genetic mouse models of psychiatric disorders. J. Psychiatr. Res. *55*, 87-95.

Haarhuis, J.H., Elbatsh, A.M., and Rowland, B.D. (2014). Cohesin and its regulation: on the logic of X-shaped chromosomes. Dev. Cell *31*, 7-18.

Haarhuis, J.H.I., van der Weide, R.H., Blomen, V.A., Yanez-Cuna, J.O., Amendola, M., van Ruiten, M.S., Krijger, P.H.L., Teunissen, H., Medema, R.H., van Steensel, B.*, et al.* (2017). The Cohesin Release Factor WAPL Restricts Chromatin Loop Extension. Cell *169*, 693-707 e614.

Hara, K., Zheng, G., Qu, Q., Liu, H., Ouyang, Z., Chen, Z., Tomchick, D.R., and Yu, H. (2014). Structure of cohesin subcomplex pinpoints direct shugoshin-Wapl antagonism in centromeric cohesion. Nat. Struct. Mol. Biol. *21*, 864-870.

Heinz, S., Benner, C., Spann, N., Bertolino, E., Lin, Y.C., Laslo, P., Cheng, J.X., Murre, C., Singh, H., and Glass, C.K. (2010). Simple combinations of lineage-determining transcription factors prime cis-regulatory elements required for macrophage and B cell identities. Mol. Cell *38*, 576-589.

Hubler, Z., Allimuthu, D., Bederman, I., Elitt, M.S., Madhavan, M., Allan, K.C., Shick, H.E., Garrison, E., M, T.K., Factor, D.C.*, et al.* (2018). Accumulation of 8,9-unsaturated sterols drives oligodendrocyte formation and remyelination. Nature *560*, 372-376.

Kim, Y., Shi, Z., Zhang, H., Finkelstein, I.J., and Yu, H. (2019). Human cohesin compacts DNA by loop extrusion. Science *366*, 1345-1349.

Kojic, A., Cuadrado, A., De Koninck, M., Gimenez-Llorente, D., Rodriguez-Corsino, M., Gomez-Lopez, G., Le Dily, F., Marti-Renom, M.A., and Losada, A. (2018). Distinct roles of

cohesin-SA1 and cohesin-SA2 in 3D chromosome organization. Nat. Struct. Mol. Biol. *25*, 496-504.

Langmead, B., and Salzberg, S.L. (2012). Fast gapped-read alignment with Bowtie 2. Nat. Methods *9*, 357-359.

Lazaris, C., Kelly, S., Ntziachristos, P., Aifantis, I., and Tsirigos, A. (2017). HiC-bench: comprehensive and reproducible Hi-C data analysis designed for parameter exploration and benchmarking. BMC Genomics *18*, 22.

Li, Y., Haarhuis, J.H.I., Sedeno Cacciatore, A., Oldenkamp, R., van Ruiten, M.S., Willems, L., Teunissen, H., Muir, K.W., de Wit, E., Rowland, B.D.*, et al.* (2020). The structural basis for cohesin-CTCF-anchored loops. Nature *578*, 472-476.

Liao, Y., Smyth, G.K., and Shi, W. (2014). featureCounts: an efficient general purpose program for assigning sequence reads to genomic features. Bioinformatics *30*, 923-930.

Liu, X., Zhang, Y., Chen, Y., Li, M., Zhou, F., Li, K., Cao, H., Ni, M., Liu, Y., Gu, Z.*, et al.* (2017). In Situ Capture of Chromatin Interactions by Biotinylated dCas9. Cell *170*, 1028-1043 e1019.

Lopez-Delisle, L., Rabbani, L., Wolff, J., Bhardwaj, V., Backofen, R., Gruning, B., Ramirez, F., and Manke, T. (2020). pyGenomeTracks: reproducible plots for multivariate genomic data sets. Bioinformatics.

Luecken, M.D., and Theis, F.J. (2019). Current best practices in single-cell RNA-seq analysis: a tutorial. Mol Syst Biol *15*, e8746.

Mannini, L., Cucco, F., Quarantotti, V., Krantz, I.D., and Musio, A. (2013). Mutation spectrum and genotype-phenotype correlation in Cornelia de Lange syndrome. Hum. Mutat. *34*, 1589-1596.

Marques, S., van Bruggen, D., Vanichkina, D.P., Floriddia, E.M., Munguba, H., Varemo, L., Giacomello, S., Falcao, A.M., Meijer, M., Bjorklund, A.K., *et al.* (2018). Transcriptional Convergence of Oligodendrocyte Lineage Progenitors during Development. Dev. Cell *46*, 504-517 e507.

Marques, S., Zeisel, A., Codeluppi, S., van Bruggen, D., Mendanha Falcao, A., Xiao, L., Li, H., Haring, M., Hochgerner, H., Romanov, R.A., *et al.* (2016). Oligodendrocyte heterogeneity in the mouse juvenile and adult central nervous system. Science *352*, 1326-1329.

Martincorena, I., and Campbell, P.J. (2015). Somatic mutation in cancer and normal cells. Science *349*, 1483-1489.

Marton, R.M., Miura, Y., Sloan, S.A., Li, Q., Revah, O., Levy, R.J., Huguenard, J.R., and Pasca, S.P. (2019). Differentiation and maturation of oligodendrocytes in human three-dimensional neural cultures. Nat. Neurosci. *22*, 484-491.

Mathys, H., Davila-Velderrain, J., Peng, Z., Gao, F., Mohammadi, S., Young, J.Z., Menon, M., He, L., Abdurrob, F., Jiang, X., *et al.* (2019). Single-cell transcriptomic analysis of Alzheimer's disease. Nature *570*, 332-337.

McDonald, J.G., Smith, D.D., Stiles, A.R., and Russell, D.W. (2012). A comprehensive method for extraction and quantitative analysis of sterols and secosteroids from human plasma. J. Lipid Res. *53*, 1399-1409.

Mitew, S., Hay, C.M., Peckham, H., Xiao, J., Koenning, M., and Emery, B. (2014). Mechanisms regulating the development of oligodendrocytes and central nervous system myelin. Neuroscience *276*, 29-47.

Moore, M.J., and Proudfoot, N.J. (2009). Pre-mRNA processing reaches back to transcription and ahead to translation. Cell *136*, 688-700.

Pan, H., Jin, M., Ghadiyaram, A., Kaur, P., Miller, H.E., Ta, H.M., Liu, M., Fan, Y., Mahn, C., Gorthi, A.*, et al.* (2020). Cohesin SA1 and SA2 are RNA binding proteins that localize to RNA containing regions on DNA. Nucleic Acids Res. *48*, 5639-5655.

Piche, J., Van Vliet, P.P., Puceat, M., and Andelfinger, G. (2019). The expanding phenotypes of cohesinopathies: one ring to rule them all! Cell Cycle *18*, 2828-2848.

Porter, H., Li, Y., Varsally, W., Neguembor, M.V., Beltran, M., Pezic, D., Martin, L., Cornejo, M.T., Bhamra, A., Surinova, S.*, et al.* (2021). STAG proteins promote cohesin ring loading at R-loops. bioRxiv, 2021.2002.2020.432055.

Rao, S.S.P., Huang, S.C., Glenn St Hilaire, B., Engreitz, J.M., Perez, E.M., Kieffer-Kwon, K.R., Sanborn, A.L., Johnstone, S.E., Bascom, G.D., Bochkov, I.D.*, et al.* (2017). Cohesin Loss Eliminates All Loop Domains. Cell *171*, 305-320 e324.

Remeseiro, S., Cuadrado, A., Carretero, M., Martinez, P., Drosopoulos, W.C., Canamero, M., Schildkraut, C.L., Blasco, M.A., and Losada, A. (2012). Cohesin-SA1 deficiency drives aneuploidy and tumourigenesis in mice due to impaired replication of telomeres. EMBO J. *31*, 2076-2089.

Remeseiro, S., Cuadrado, A., Kawauchi, S., Calof, A.L., Lander, A.D., and Losada, A. (2013a). Reduction of Nipbl impairs cohesin loading locally and affects transcription but not cohesion-dependent functions in a mouse model of Cornelia de Lange Syndrome. Biochim. Biophys. Acta *1832*, 2097-2102.

Remeseiro, S., Cuadrado, A., and Losada, A. (2013b). Cohesin in development and disease. Development *140*, 3715-3718.

Robinson, M.D., McCarthy, D.J., and Smyth, G.K. (2010). edgeR: a Bioconductor package for differential expression analysis of digital gene expression data. Bioinformatics *26*, 139-140.

Ross-Innes, C.S., Stark, R., Teschendorff, A.E., Holmes, K.A., Ali, H.R., Dunning, M.J., Brown, G.D., Gojis, O., Ellis, I.O., Green, A.R., *et al.* (2012). Differential oestrogen receptor binding is associated with clinical outcome in breast cancer. Nature *481*, 389-393.

Saher, G., Brugger, B., Lappe-Siefke, C., Mobius, W., Tozawa, R., Wehr, M.C., Wieland, F., Ishibashi, S., and Nave, K.A. (2005). High cholesterol level is essential for myelin membrane growth. Nat. Neurosci. *8*, 468-475.

Saunders, A., Macosko, E.Z., Wysoker, A., Goldman, M., Krienen, F.M., de Rivera, H., Bien, E., Baum, M., Bortolin, L., Wang, S., *et al.* (2018). Molecular Diversity and Specializations among the Cells of the Adult Mouse Brain. Cell *174*, 1015-1030 e1016.

Schwarzer, W., Abdennur, N., Goloborodko, A., Pekowska, A., Fudenberg, G., Loe-Mie, Y., Fonseca, N.A., Huber, W., Haering, C.H., Mirny, L., *et al.* (2017). Two independent modes of chromatin organization revealed by cohesin removal. Nature *551*, 51-56.

Shi, Z., Gao, H., Bai, X.C., and Yu, H. (2020). Cryo-EM structure of the human cohesin-NIPBL-DNA complex. Science *368*, 1454-1459.

Soardi, F.C., Machado-Silva, A., Linhares, N.D., Zheng, G., Qu, Q., Pena, H.B., Martins, T.M.M., Vieira, H.G.S., Pereira, N.B., Melo-Minardi, R.C., *et al.* (2017). Familial STAG2 germline mutation defines a new human cohesinopathy. NPJ Genom. Med. *2*, 7.

Stuart, T., Butler, A., Hoffman, P., Hafemeister, C., Papalexi, E., Mauck, W.M., 3rd, Hao, Y., Stoeckius, M., Smibert, P., and Satija, R. (2019). Comprehensive Integration of Single-Cell Data. Cell *177*, 1888-1902 e1821.

Thakurela, S., Garding, A., Jung, R.B., Muller, C., Goebbels, S., White, R., Werner, H.B., and Tiwari, V.K. (2016). The transcriptome of mouse central nervous system myelin. Sci. Rep. *6*, 25828.

Tronche, F., Kellendonk, C., Kretz, O., Gass, P., Anlag, K., Orban, P.C., Bock, R., Klein, R., and Schutz, G. (1999). Disruption of the glucocorticoid receptor gene in the nervous system results in reduced anxiety. Nat. Genet. *23*, 99-103.

Tsirigos, A., Haiminen, N., Bilal, E., and Utro, F. (2012). GenomicTools: a computational platform for developing high-throughput analytics in genomics. Bioinformatics *28*, 282-283.

Uhlmann, F. (2016). SMC complexes: from DNA to chromosomes. Nat. Rev. Mol. Cell Biol. *17*, 399-412.

van Tilborg, E., van Kammen, C.M., de Theije, C.G.M., van Meer, M.P.A., Dijkhuizen, R.M., and Nijboer, C.H. (2017). A quantitative method for microstructural analysis of myelinated axons in the injured rodent brain. Sci. Rep. *7*, 16492.

Vian, L., Pekowska, A., Rao, S.S.P., Kieffer-Kwon, K.R., Jung, S., Baranello, L., Huang, S.C., El Khattabi, L., Dose, M., Pruett, N.*, et al.* (2018). The Energetics and Physiological Impact of Cohesin Extrusion. Cell *175*, 292-294.

Vuilleumier, N., Kovari, E., Michon, A., Hof, P.R., Mentenopoulos, G., Giannakopoulos, P., and Bouras, C. (2002). Neuropathological analysis of an adult case of the Cornelia de Lange syndrome. Acta Neuropathol. *104*, 327-332.

Williamson, J.M., and Lyons, D.A. (2018). Myelin Dynamics Throughout Life: An Ever-Changing Landscape? Front. Cell Neurosci. *12*, 424.

Wingett, S. (2011). FastQ Screen: quality control tool to screen a library of sequences in FastQ format against a set of sequence databases. .

Wolf, N.I., Ffrench-Constant, C., and van der Knaap, M.S. (2021). Hypomyelinating leukodystrophies - unravelling myelin biology. Nat. Rev. Neurol. *17*, 88-103.

Wutz, G., Ladurner, R., St Hilaire, B.G., Stocsits, R.R., Nagasaka, K., Pignard, B., Sanborn, A., Tang, W., Varnai, C., Ivanov, M.P., *et al.* (2020). ESCO1 and CTCF enable formation of long chromatin loops by protecting cohesin(STAG1) from WAPL. eLife *9*.

Wutz, G., Varnai, C., Nagasaka, K., Cisneros, D.A., Stocsits, R.R., Tang, W., Schoenfelder, S., Jessberger, G., Muhar, M., Hossain, M.J., *et al.* (2017). Topologically associating domains and chromatin loops depend on cohesin and are regulated by CTCF, WAPL, and PDS5 proteins. EMBO J. *36*, 3573-3599.

Yatskevich, S., Rhodes, J., and Nasmyth, K. (2019). Organization of Chromosomal DNA by SMC Complexes. Annu. Rev. Genet. *53*, 445-482.

Zeisel, A., Hochgerner, H., Lonnerberg, P., Johnsson, A., Memic, F., van der Zwan, J., Haring, M., Braun, E., Borm, L.E., La Manno, G., *et al.* (2018). Molecular Architecture of the Mouse Nervous System. Cell *174*, 999-1014 e1022.

Zhang, Y., Liu, T., Meyer, C.A., Eeckhoute, J., Johnson, D.S., Bernstein, B.E., Nusbaum, C., Myers, R.M., Brown, M., Li, W., *et al.* (2008). Model-based analysis of ChIP-Seq (MACS). Genome Biol. *9*, R137.

Zheng, G., and Yu, H. (2015). Regulation of sister chromatid cohesion during the mitotic cell cycle. Sci. China Life Sci. *58*, 1089-1098.

Zywitza, V., Misios, A., Bunatyan, L., Willnow, T.E., and Rajewsky, N. (2018). Single-Cell Transcriptomics Characterizes Cell Types in the Subventricular Zone and Uncovers Molecular Defects Impairing Adult Neurogenesis. Cell Rep. *25*, 2457-2469 e2458.

Figures

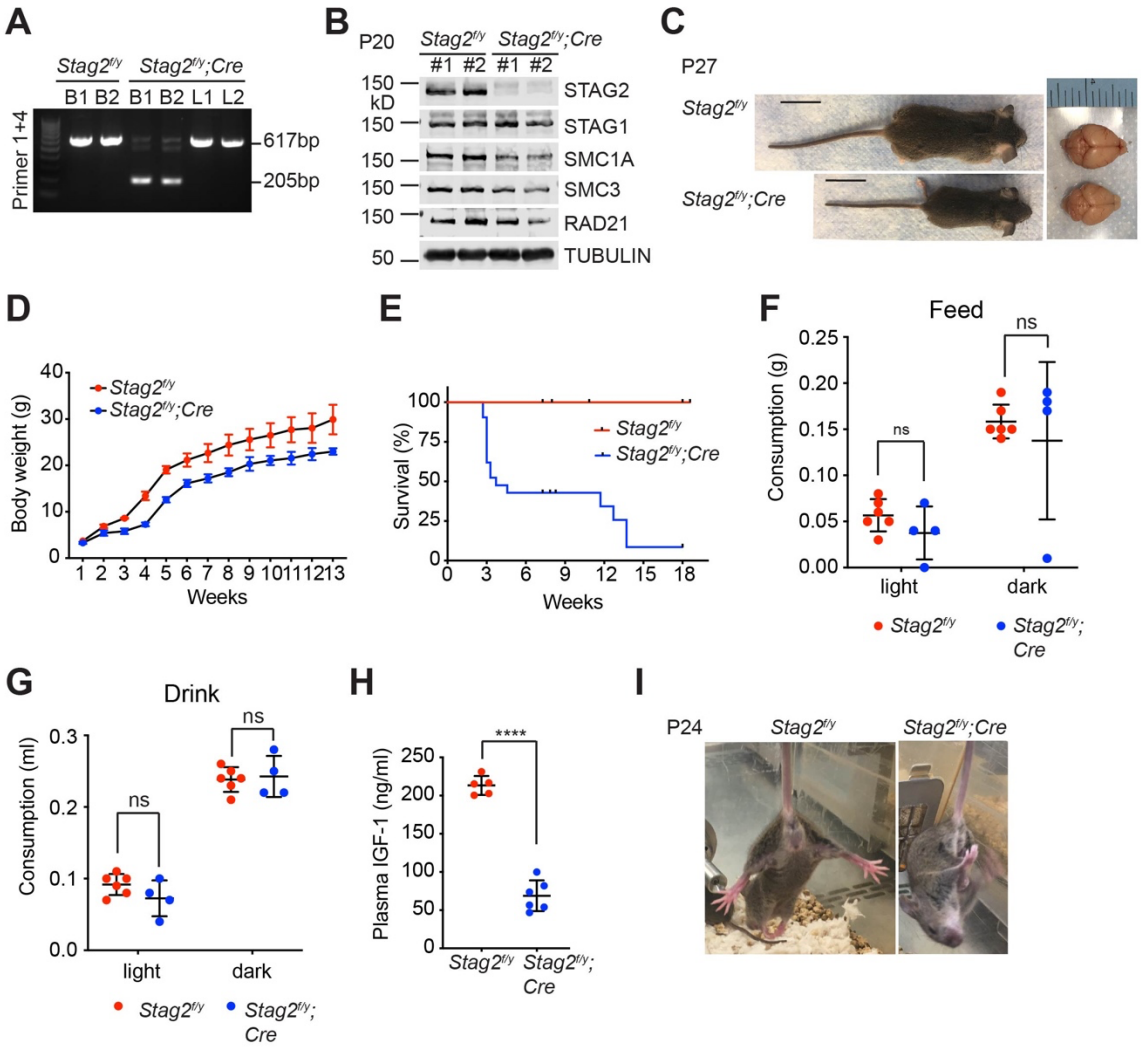

Figure 1. *Stag2* ablation in the mouse nervous system causes growth retardation and neurological defects.

(A) PCR analysis of genomic DNA extracted from brains (BR) or livers (LV) of indicated mice.

(B) Immunoblots of brain lysates of *Stag2*$^{f/y}$ and *Stag2*$^{f/y}$*;Cre* mice.

(C) Representative images of *Stag2*$^{f/y}$ and *Stag2*$^{f/y}$*;Cre* mice. Scale bar = 2 cm.

(D) Body weight of *Stag2*$^{f/y}$ and *Stag2*$^{f/y}$*;Cre* mice at different age. Mean ± SD of at least three mice of the same age.

(E) Survival curves of *Stag2*$^{f/y}$ (n = 12) and *Stag2*$^{f/y}$*;Cre* (n = 21) mice.

(F,G) Food (F) and water (G) consumption of 7- to 8-week-old *Stag2*$^{f/y}$ (n = 6) and *Stag2*$^{f/y}$*;Cre* (n = 4) mice. Mean ± SD; ns, not significant.

(H) Plasma IGF-1 levels of two-month-old *Stag2*$^{f/y}$ (n = 5) and *Stag2*$^{f/y}$*;Cre* (n = 6) mice. Mean ± SD; ****$p < 0.0001$

(I) Representative images of limb-clasping responses of *Stag2*$^{f/y}$ and *Stag2*$^{f/y}$*;Cre* mice.

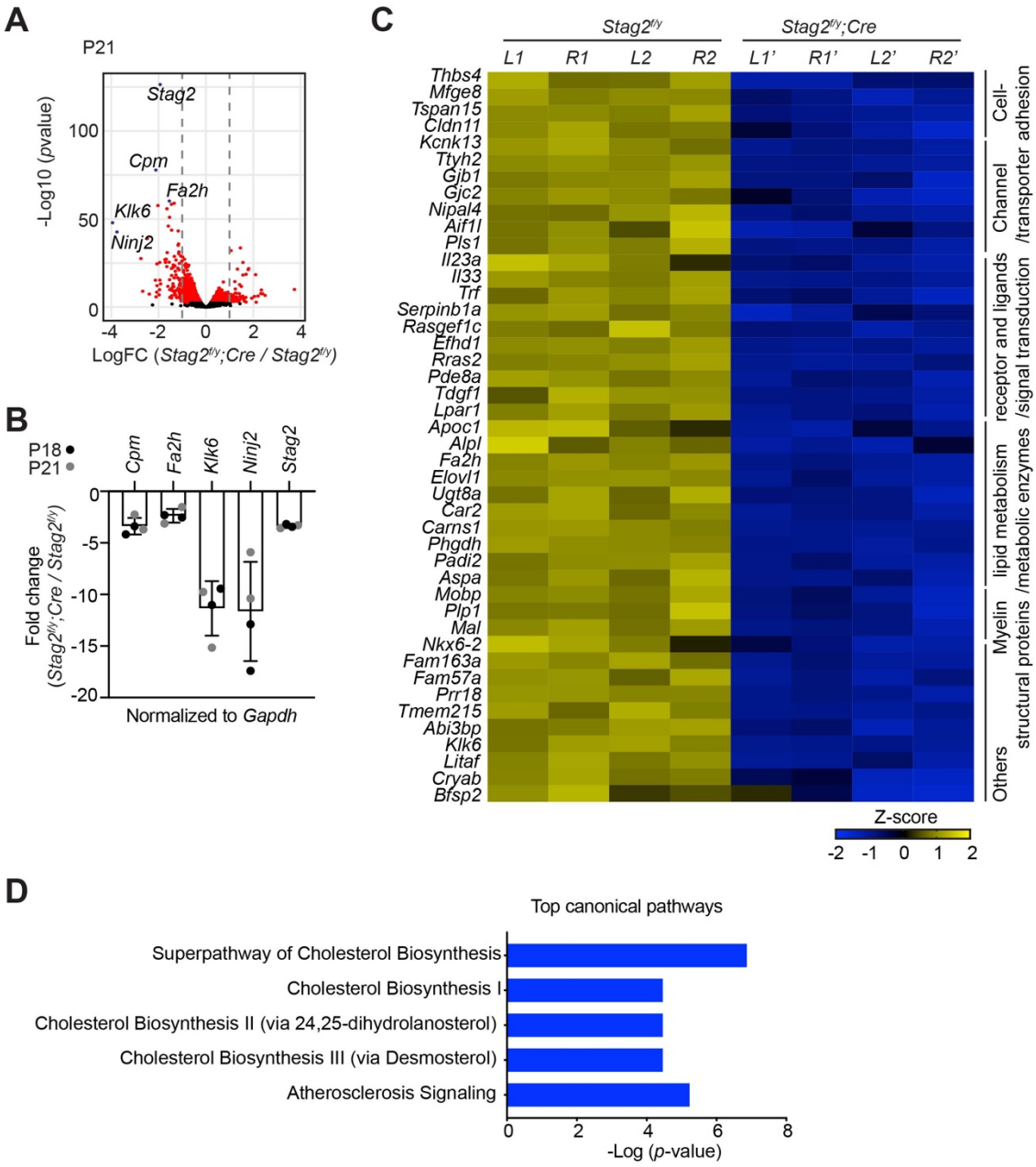

Figure 2. *Stag2* ablation in mouse brains downregulates the expression of myelin genes.

(A) Volcano plot of bulk RNA sequencing results of *Stag2*$^{f/y}$ and *Stag2*$^{f/y}$*;Cre* brain extracts. Top differentially expressed genes (DEGs) are colored blue and labeled. n = 4 pairs of P21 *Stag2*$^{f/y}$ and *Stag2*$^{f/y}$*;Cre* brain hemispheres were used for the comparison.

(B) RT-qPCR analysis of the top downregulated genes in the brain extracts. n = 4 pairs of *Stag2$^{f/y}$* and *Stag2$^{f/y}$;Cre* littermates were used. Mean ± SD.

(C) Heatmap of the expression of myelin-enriched genes that were down-regulated by more than two folds in *Stag2$^{f/y}$;Cre* brains. *L1* and *R1*, left and right brain hemispheres of the *Stag2$^{f/y}$#1* mouse. *L2* and *R2*, left and right brain hemispheres of the *Stag2$^{f/y}$#2* mouse. *L1'* and *R1'*, left and right brain hemispheres of the *Stag2$^{f/y}$;Cre #1* mouse. *L2'* and *R2'*, left and right brain hemispheres of the *Stag2$^{f/y}$;Cre#2* mouse. The biological pathways of these genes are labeled on the right.

(D) Top canonical pathways identified by ingenuity pathway analysis (IPA) of the DEGs.

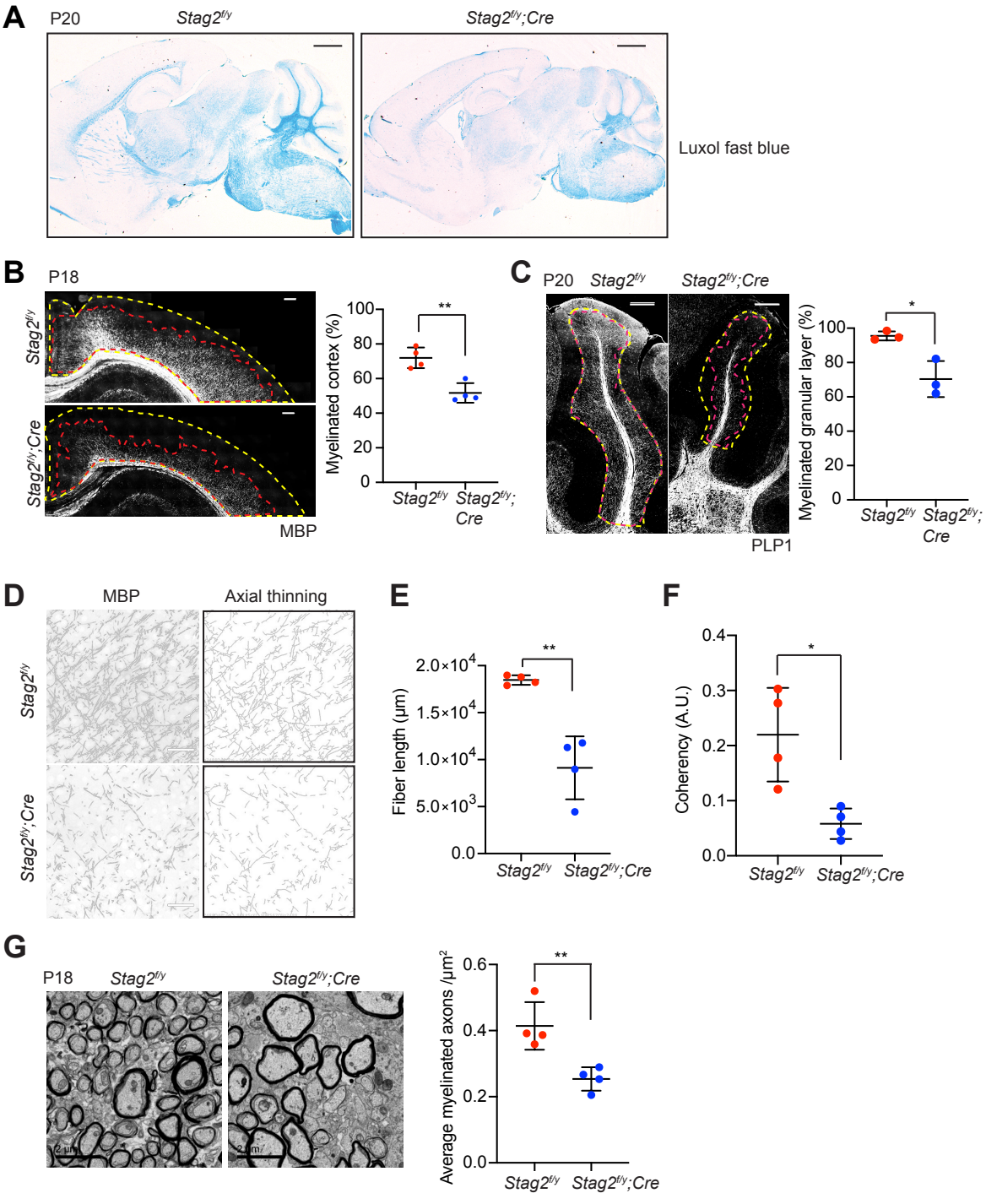

Figure 3. *Stag2* ablation in the nervous system compromises myelination during early postnatal development.

(A) Luxol fast blue staining of the sagittal sections of *Stag2*$^{f/y}$ and *Stag2*$^{f/y}$*;Cre* brains. n = 3 animals per genotype. Scale bar = 1 mm.

(B) Immunohistochemistry staining with the anti-MBP antibody in the cerebral cortex (left panel). Antibody-stained areas and DAPI staining regions are marked with red and yellow dashed lines, respectively. Scale bar = 200 μm. Quantification of the percentage of the myelinated cortex is shown in the right panel. n = 4 pairs of *Stag2*$^{f/y}$ and *Stag2*$^{f/y}$*;Cre* littermates were used (P18 or P21) for the comparison. **p < 0.01; Mean ± SD.

(C) Immunohistochemistry staining with the anti-PLP1 antibody in the cerebellum (left panel). Antibody-stained areas and DAPI staining regions are marked with red and yellow dashed lines, respectively. Scale bar = 200 μm. Quantification of the percentage of the myelinated cerebellum granular layer is shown in the right panel. n = 3 pairs of *Stag2*$^{f/y}$ and *Stag2*$^{f/y}$*;Cre* littermates were used (P20 or P25) for the comparison. *p < 0.05; Mean ± SD.

(D) Higher magnification images (left panel) of the immunohistochemistry staining with the anti-MBP antibody in (B). Images processed through axial thinning are shown in the right panel. Scale bar = 50 μm.

(E,F) Total fiber length (E) and fiber coherency (F) measured using the processed images in (D). n = 4 pairs of *Stag2*$^{f/y}$ and *Stag2*$^{f/y}$*;Cre* littermates were used (P18 or P21). *p < 0.05, **p < 0.01; Mean ± SD.

(G) Transmission electron microscopy images of the optic nerves (left panel). Scale bar = 2 μm. Quantification of myelinated axon distributions is shown in the right panel. n = 4 pairs of P18 *Stag2*$^{f/y}$ and *Stag2*$^{f/y}$*;Cre* littermates were used. n ≥ 10 fields of each mouse were taken, and the average distribution of myelinated axons were calculated for each mouse and plotted. **p < 0.01; Mean ± SD.

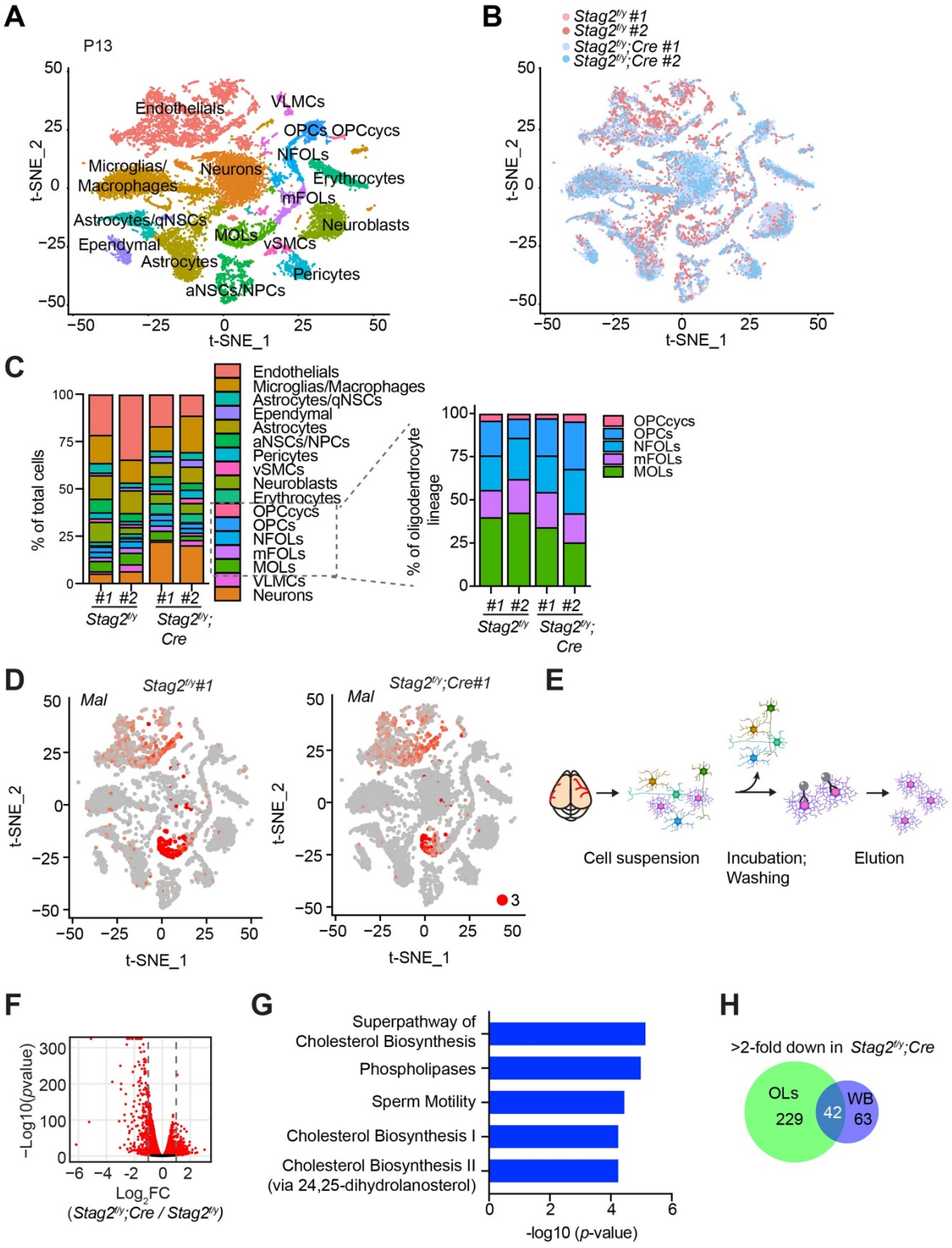

Figure 4. Deletion of *Stag2* in mouse brains causes differentiation delay and transcriptional changes in oligodendrocytes.

(A) *t*-SNE plot of cell clusters in *Stag2*$^{f/y}$ and *Stag2*$^{f/y}$*;Cre* forebrains analyzed by single-cell RNA-seq (scRNA-seq). n = 2 mice of each genotype were used in the scRNA-seq analysis. aNSCs/NPCs, active neural stem cells or neural progenitor cells; Astrocytes/qNSCs, astrocytes or quiescent neural stem cells; OPCcycs, cycling oligodendrocyte (OL) progenitor cells; OPCs, OL progenitor cells; NFOLs, newly formed OLs; mFOLs, myelin-forming OLs; MOLs, matured OLs; VLMCs, vascular and leptomeningeal cells; vSMCs, vascular smooth muscle cells.

(B) *t*-SNE clustering as in (A) but colored by genotype.

(C) Left panel: cell type composition and percentage as colored in (A). Right panel: percentage of cell clusters of the oligodendrocyte lineage.

(D) FeaturePlot of a representative gene (*Mal*) specifically suppressed in MOLs of *Stag2*$^{f/y}$*;Cre* forebrains. A maximum cutoff of 3 was used.

(E) Experimental scheme of the magnetic-activated cell sorting (MACS) of primary OLs.

(F) Volcano plot of bulk RNA-seq results of *Stag2*$^{f/y}$ and *Stag2*$^{f/y}$*;Cre* primary OLs.

(G) Top canonical pathways identified by IPA of the DEGs in (F).

(H) Commons DEGs shared between bulk RNA-seq analyses of the whole brains (WB) and primary OLs.

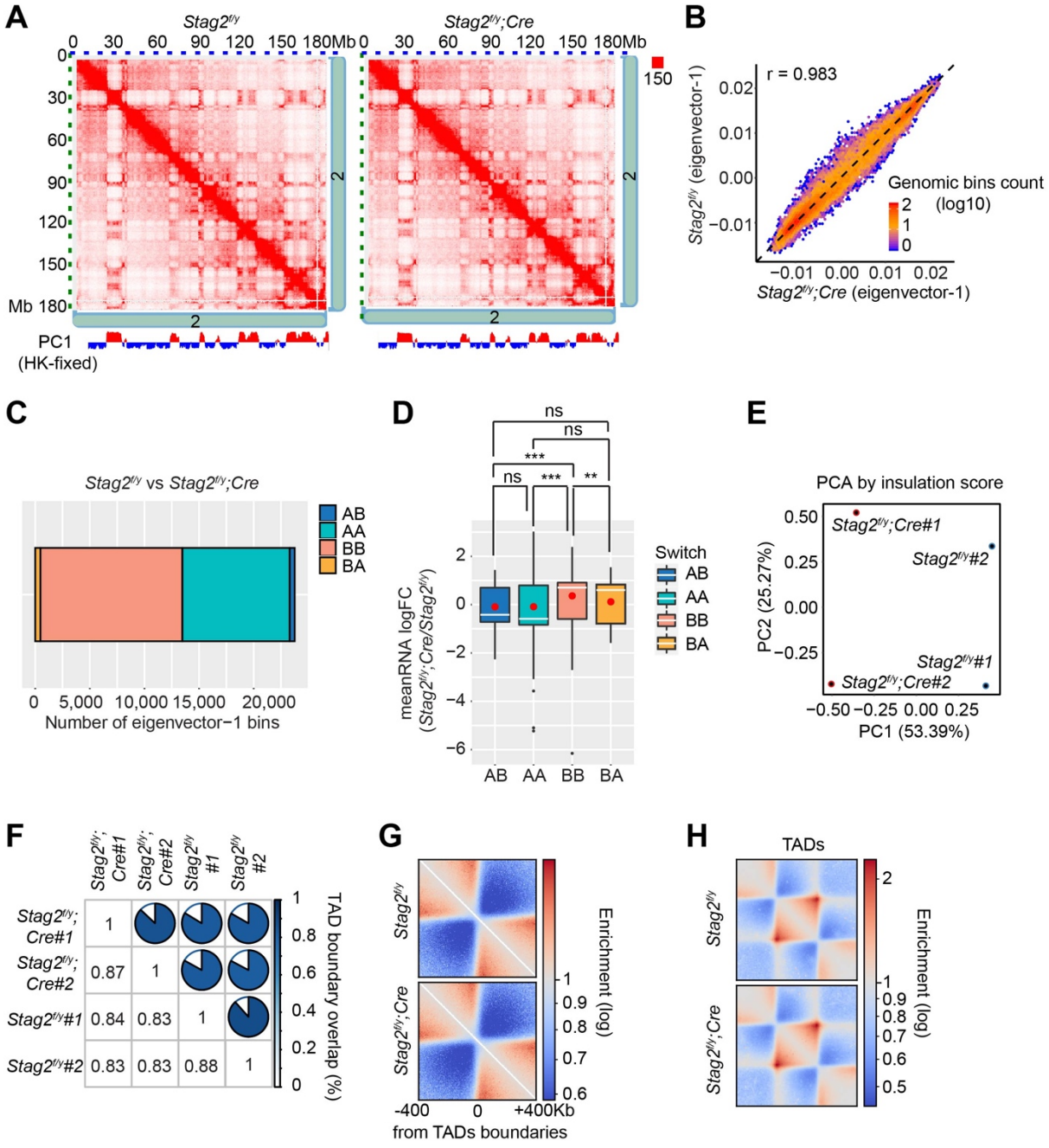

Figure 5. Loss of *Stag2* does not alter compartments and TADs in oligodendrocytes.

(A) Representative snapshots of balanced Hi-C contact matrices of chromosome 2. Tracks of eigenvector-1 fixed with housekeeping genes are shown below, with A and B compartments shown in red and blue, respectively.

(B) Hexbin plot of eigenvector-1 for genomic bins (100 kb) in *Stag2*$^{f/y}$ and *Stag2*$^{f/y}$*;Cre* oligodendrocytes (OLs).

(C) Chromatin bins were classified into four categories based on the eigenvector sign and whether it has switched with a delta bigger than 1.5. AB, changing from compartment A in *Stag2*$^{f/y}$ to compartment B in *Stag2*$^{f/y}$*;Cre*; BA, from B in *Stag2*$^{f/y}$ to A in *Stag2*$^{f/y}$*;Cre*; AA, A in both *Stag2*$^{f/y}$ and *Stag2*$^{f/y}$*;Cre*; BB, B in both *Stag2*$^{f/y}$ and *Stag2*$^{f/y}$*;Cre*.

(D) Boxplot of averaged gene expression change of DEGs (RNA logFC cutoff of ± 0.58) inside each genomic bin. Bins counted: AA, 1646; AB, 56; BA, 69; BB, 910. Red dots represent the mean value. An unpaired Wilcoxon test was used for the statistical analysis. *$p < 0.05$; **$p < 0.01$; ***$p < 0.001$; ns, not significant.

(E) Principal component analysis (PCA) plot of the insulation score.

(F) Overlaps of TAD boundaries between genotypes and biological replicates.

(G) Pile-up analysis of TAD boundary-centered local structure flanked by 400 kb chromatin regions.

(H) Pile-up analysis of TAD local structure rescaled to an equal size.

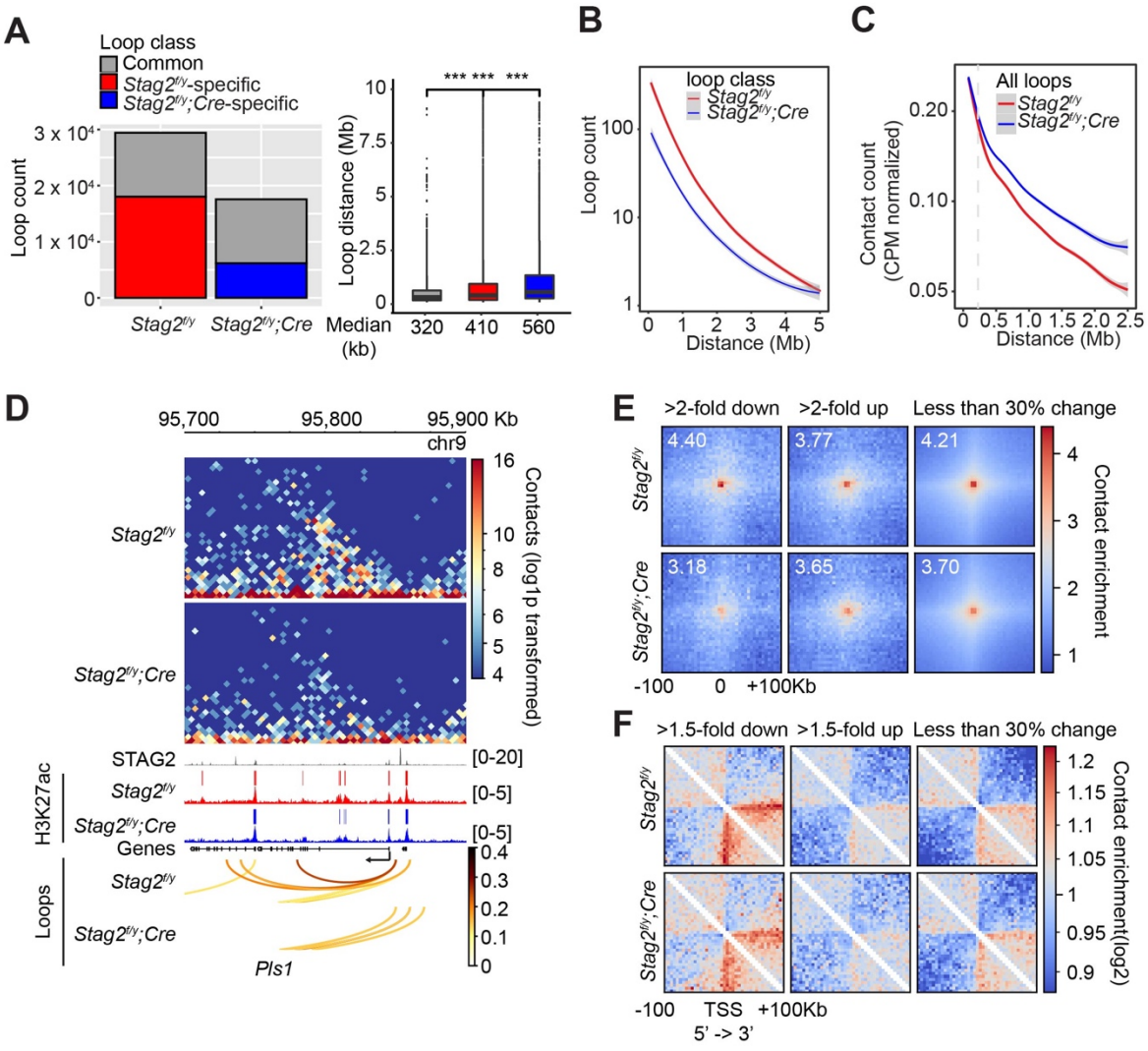

Figure 6. *Stag2* deletion impairs the formation of total and promoter-anchored loops in oligodendrocytes.

(A) Loop counts (left panel) and length (right panel) in the indicated categories of *Stag2$^{f/y}$* and *Stag2$^{f/y}$;Cre* oligodendrocytes (OLs).

(B) Loop counts plotted against loop length (from 0 to 5 Mb) of *Stag2$^{f/y}$* and *Stag2$^{f/y}$;Cre* OLs.

(C) Normalized contact counts for loops across different genomic distances in *Stag2*$^{f/y}$ and *Stag2*$^{f/y}$*;Cre* OLs.

(D) Representative snapshots of contact maps at the *Pls1* gene locus. Tracks and narrow peaks from STAG2 and H3K27ac ChIP-seq as well as the loops are plotted below. Transcription direction is indicated by the black arrow.

(E) Pile-up analysis of loop "dots"-centered local maps for the promoter-anchored loops of genes in the indicated categories. The maps are balanced, normalized by distance, and plotted at 5 kb resolution. The numbers indicate the enrichment of the central pixel over the upper left and bottom right corners.

(F) Pile-up analysis of the local contact maps centered around the transcription start site (TSS) of genes in the indicated categories. Transcription directions are indicated below. 1,000 stable genes are chosen randomly and used for the analysis. The maps are balanced, normalized by distance, and plotted at 5kb resolution. Diagonal pixels are omitted.

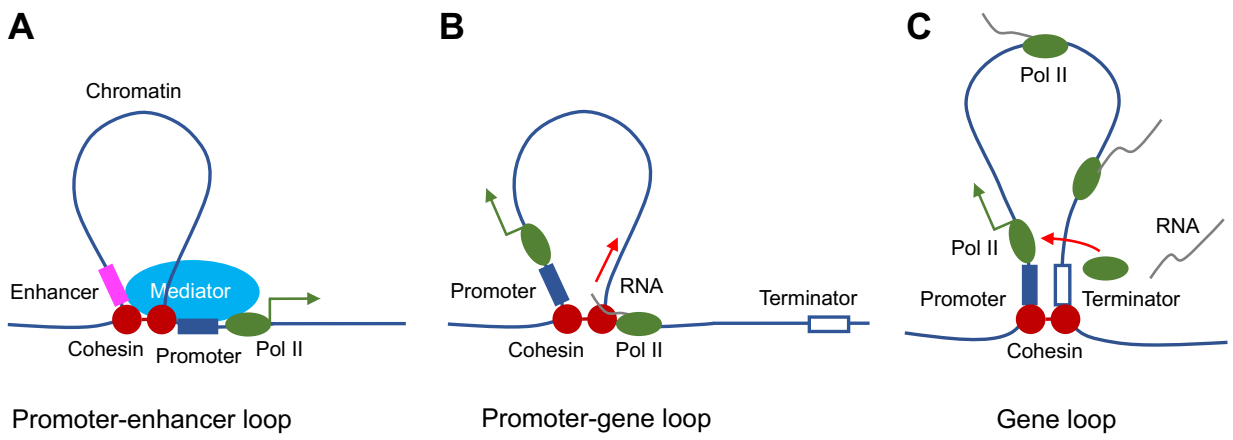

Figure 7. Proposed roles of STAG2-cohesin-mediated loop extrusion during transcription in oligodendrocytes.

(A) STAG2-cohesin-mediated chromosome looping connects the enhancer and the promoter, thus facilitating interactions among oligodendrocyte-specific transcription factors, the mediator complex, and the general transcription machinery including RNA polymerase II.

(B) STAG2-cohesin travels along the gene body via transcription-coupled loop extrusion to facilitate pre-mRNA processing.

(C) STAG2-cohesin mediates the formation of gene loops that bring the terminator close to the promoter and facilitate Pol II recycling for multiple rounds of transcription.